J. Min. Metall. Sect. B-Metall. 60 (3) (2024) 461 - 470

Journal of Mining and Metallurgy, Section B: Metallurgy

ANALYSIS OF PREMATURE CRACKING CAUSES OF ASTM A213-T12 SUPERHEATER TUBE

J.-G. Chen [a, *], J. Dong [a], H.-W. Zhang [b], Y.-X. Huang [b], Q.-J. Ma [b], Y.-S. Wei [b], H.-S. Ma [c]

[a] School of Mechanical Engineering, Tianjin Sino-German University of Applied Sciences, Tianjin, PR China
[b] Tianjin Special Equipment Inspection Institute, Tianjin, PR China
[c] Tianjin Bridge Welding Materials Group Co., Ltd, Tianjin, PR China

(Received 21 May 2024; Accepted 25 December 2024)

Abstract

The failure behavior of the superheater tube made of ASTM A213-T12 steel was studied. The microstructure and hardness at different positions of the tube, the element distribution at the crack location, and the morphology and phase composition of the corrosion layer were analyzed by optical microscopy (OM), microhardness tester, scanning electron microscopy (SEM), and X-ray diffractometer (XRD). The results show that the pearlite undergoes spheroidization at the fracture site and the hardness is significantly reduced compared to the normal position. The failure is closely linked to corrosion and creep. On the one hand, sulfur corrosion and oxidation corrosion occur on the outer layer of the superheater tube, which greatly reduces the thickness of the tube. On the other hand, the creep resistance of the tube is significantly reduced by the thinning. There are numerous creep voids in the microstructure at the failure site. Meanwhile, oxygen can diffuse into the voids to promote oxidation corrosion.

Keywords: *Superheater tube; Failure analysis; Creep; Corrosion; Microstructure*

1. Introduction

Boiler is one of the key equipment of a power generation unit, which converts water into superheated steam and then transports it to a turbine for power generation. A boiler is composed of multiple different components, such as economizer, water-cooled wall, superheater, and reheater. The function of a superheater is to heat saturated steam into superheated steam, reduce smoke exhaust losses, and improve boiler thermal efficiency. The steam inside the tube is superheated through heat exchange with the flue gas in the shell side. The high-temperature superheater tube is the component with the highest operating temperature and the most complex operating conditions in coal-fired power unit boilers. During operation, the superheater tube experiences high temperatures from the external environment, as well as high pressures and temperatures from the inside, often accompanied by failure [1-3]. The failure of the superheater tube can lead to unplanned shutdown or low load operation of the unit, seriously affecting the safe operation and economic benefits of the boiler. The failure mode of superheater tubes is relatively complex and vary under different service conditions. Kochmański et al. [4] studied the failure of ASTM T22 superheater tubes. The cause of the failure was found to be an increase in the thickness of the oxygen layer on the inner surface of the tube, leading to overheating of the tube. Wang et al. [5] studied the failure of 12Cr1MoV superheater tubes during long-term service and confirmed that creep is the cause of tube rupture. Liu et al. [6] found that sulfurization-oxidation corrosion was the cause of the failure of Incoloy 800HT superheater tube. Li et al. [7] analyzed the cracking reasons of ASTM SA210 superheater tubes and found that stress corrosion cracking was the cause of tube failure. Therefore, the failure mode of the superheater tube is directly related to the material of the tube and the service conditions of the tube.

Cr-Mo heat-resistant steels are widely used in components such as steam chests, valve bodies, superheaters and reheaters of power generation units due to their excellent resistance to high-temperature oxidation and high-temperature creep [8-10]. As a type of Cr-Mo low alloy heat-resistant steel, the microstructure of ASTM A213-T12 steel is composed of ferrite and pearlite [11]. ASTM A213-T12 steel is developed in the 20th century and has been the main heat-resistant steel used in power plants. It is usually

Corresponding author: chenjianguo@tsguas.edu.cn

https://doi.org/10.2298/JMMB240521037C

used after normalizing and tempering heat treatment. The improvement in mechanical properties, especially high-temperature performance, of ASTM A213-T12 steel compared to carbon steel is attributed to the introduction of Cr and Mo. Typically, the high creep resistance of ASTM A213-T12 steel mainly comes from two aspects: one is the matrix strengthening from the Cr and Mo, and the other is the dispersion strengthening from the fine carbides formed by the same elements, providing pinning effect for grain boundaries and dislocations [12]. ASTM A213-T12 steel has always been the mainstream material used for superheaters with temperatures below 560 °C in power plants operation [13]. Up to now, many in-service power generation units are still using ASTM A213-T12 steel.

This paper explores a boiler superheater tube cracking incident that occurred in a certain thermal power plant, and analyzes the failure mechanism. The superheater tube is made of ASTM A213-T12 steel and ruptured after approximately 9.5 months (283 days) of service. The failed superheater tube is located in the final superheating zone of a pulverized coal-fired boiler, with water vapor inside and flue gas outside. The outer diameter of the tube is 32.2 mm and the inner diameter is 20 mm. The working temperature and pressure of the tube are 500 °C and 12.5 MPa. The research results will provide a reference for similar failure analysis of superheater tubes. More importantly, it can also provide preventive measures to prevent similar failures from happening again in the future.

2. Materials and experiments

The failed superheater tube came from the final superheater. It was analyzed by means of chemical composition testing, size measurement, hardness measurement, optical microscopy (OM), scanning electron microscopy (SEM), energy dispersive spectrometer (EDS) and X-ray diffractometer (XRD). The chemical composition of the superheater tube is determined using an Agilent 5100VDV inductively coupled plasma (ICP) emission spectrometer and a Shanghai Kaide HCS-140 infrared carbon and sulfur analyzer. Determine the material of the superheater tube by comparing the measured chemical composition with the standard and considering the service environment of the tube. The thickness of the tube at the failed and normal positions was measured along the direction of the tube crack by a vernier caliper. Take specimens for microhardness testing and microstructure detection from the thinnest crack and the normal positions of the tube. The cold-set specimens were polished with a series of silicon carbide sandpapers before polishing and cleaning. The hardness test is carried out at the section of the thinnest cracked and normal position of the tube. The microhardness at different positions was measured using three test points with a 100g load and 20s dwell, and then the average hardness was calculated. Subsequently, the specimens were sanded and polished again, and etched in a 5% nitric acid alcohol solution. Finally, the etched specimens are placed in alcohol for ultrasonic cleaning, and then dry. An Olympus DSX510 OM was used for the metallographic detection of the specimens. The cross-sectional morphology and element distribution of the failure position of the superheater tube were observed using a Zeiss GeminiSEM500 SEM equipped with EDS. The phase composition of corrosion products on the surface of the failed superheater tube was determined by a Rigaku SmartLab-SE XRD using CuKα radiation with the 2θ from 10° to 90° and a scan rate of 20° min^{-1}.

3. Results and discussion

3.1. Chemical composition and visual examinations

The chemical composition (wt.%) of the superheater tube was tested, and the detailed values were shown in Table 1. The test result was within the range of T12 steel composition in ASTM A213/A213M-23 standard [14]. Based on the service conditions of the superheater tube and the measured chemical composition result, it is determined that the material of the superheater tube is ASTM A213-T12 steel. Fig. 1 shows the damaged superheater tube received for failure analysis. It can be observed from the figure that there is a large amount of rust on the outside of the superheater tube, and severe deformation occurs at the cracking position. The failure crack is about 50 millimeters (mm) long and appears in the shape of a fish beak. The thickness of the tube is measured along the direction of tube cracking, from the highest prominent position of the burst tube to the normal position of the tube. The test interval is about 5 mm, and the thickness values are 2.88, 3.92, 4.74, 5.46, 5.66, 6.10 mm, respectively. The thickness measurement of the tube revealed that the thinnest thickness at the failure position was 2.88 mm, while the thickness at the normal position was 6.10 mm, as shown in Fig. 2. Visual inspection confirmed corrosion and thinning of the superheater tube.

3.2. Microstructure and hardness determinations

Fig. 3 shows the OM images of the standard and failed positions of the superheater tube. It can be seen

Table 1. *Chemical composition of superheater tube in wt.%*

	C	Si	Mn	P	S	Cr	Mo	Fe
Measured value	0.149	0.248	0.584	0.0075	0.0015	0.916	0.426	Bal.
ASTM A213-T12 [14]	0.05-0.15	≤0.5	0.3-0.61	≤0.025	≤0.025	0.8-1.25	0.44-0.65	Bal.

Figure 1. *The damaged superheater tube received for failure analysis*

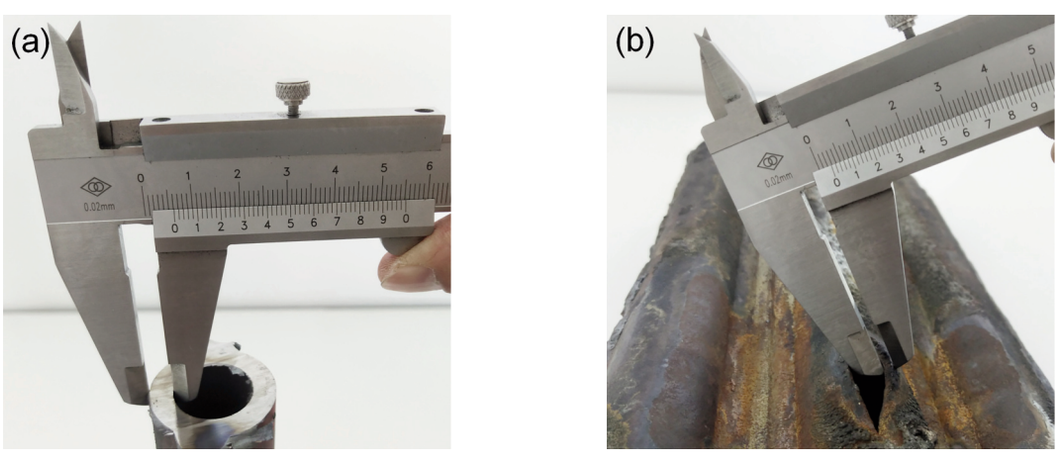

Figure 2. *Thickness measurement of the superheater tube: (a) normal position, (b) failure position*

that the microstructures are composed of white ferrite and black pearlite. The difference is that the edges and corners of the pearlite at the normal position are neat and clear, while those in the failed position become blurry and show burrs, and their colors also become lighter. This indicates that the pearlite at the failure position has undergone spheroidization. The average microhardness test results for the normal and failure positions of the superheater tube are 170 and 134 HV, respectively, which illustrates that the thinning area has lower hardness. The decrease in hardness can be explained by the spheroidization of pearlite [15].

Fig. 4 displays the cross-section's SEM and EDS mapping analysis near the outside of the superheater tube failure position. It can be observed that there are a large number of voids in the microstructure of the tube (indicated by the small red arrow). At the same time, there are also some micro-cracks. EDS detection confirmed the presence of O in the voids and cracks, further proving the existence of oxidation corrosion. This indicates that cracks and voids create some open channels below the surface for O diffusion. O element diffuses into the interior of the substrate through these open channels and reacts with iron, promoting the occurrence of tube oxidation corrosion.

In order to observe the microstructure characteristics and voids distribution of the failed tube more clearly, a high magnification SEM analysis was performed on the failure position, as illustrated in Fig. 5. The presence of voids in the microstructure was reconfirmed (as indicated by the thick red arrow in Fig. 5(a)). Multiple voids with different shapes can be

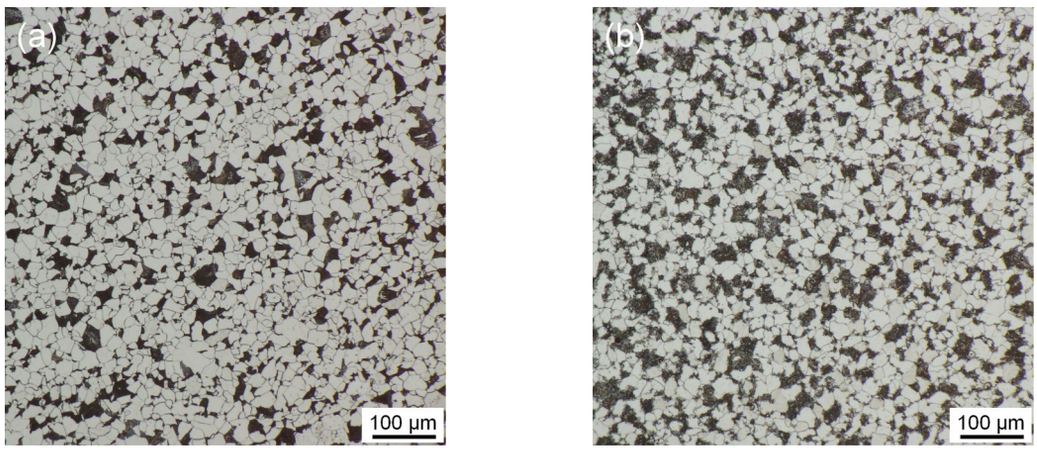

Figure 3. *OM images of the superheater tube: (a) normal position, (b) failure position*

found in the microstructure. There are elongated voids at grain boundaries, small circular voids within grains, and large voids that have already developed. Among them, the voids at grain boundaries account for the vast majority. It should be pointed out that the coalescence of adjacent voids will transform into micro-cracks [16, 17]. Meanwhile, it was further confirmed that the microstructure underwent pearlite spheroidization, as shown by the circles in Figs. 5(a), 5(b) and 5(c). The spheroidization of pearlite and the formation of micro-voids at grain boundaries or within grains both confirm the existence of creep in the structure [18]. In addition, coarsened precipitates can also be observed in the microstructure (as shown by the white arrow in Fig. 5 (c)). This further confirms the occurrence of creep [19, 20]. Therefore, combined with the deformation at the crack of the superheater tube, the presence of voids, pearlite spheroidization and coarsened precipitates in the microstructure, it can be proved that the tube has undergone creep.

After repeated cleaning of the failure position, the cleaning morphology of cracks in the microstructure was given, as depicted in Fig. 6. It is interesting that although most of the voids in the microstructure are distributed at grain boundaries (as presented in Fig. 5), the cracks do not exhibit intergranular fracture, but rather a transgranular manner, as shown in Fig. 6(d). The macroscopic plastic deformation at the crack of the superheater tube in Fig. 2(b) can also confirm the occurrence of transgranular fracture. Zhou et al. [21] also found a similar situation in the creep test of ferritic heat-resistant steel and confirmed that the

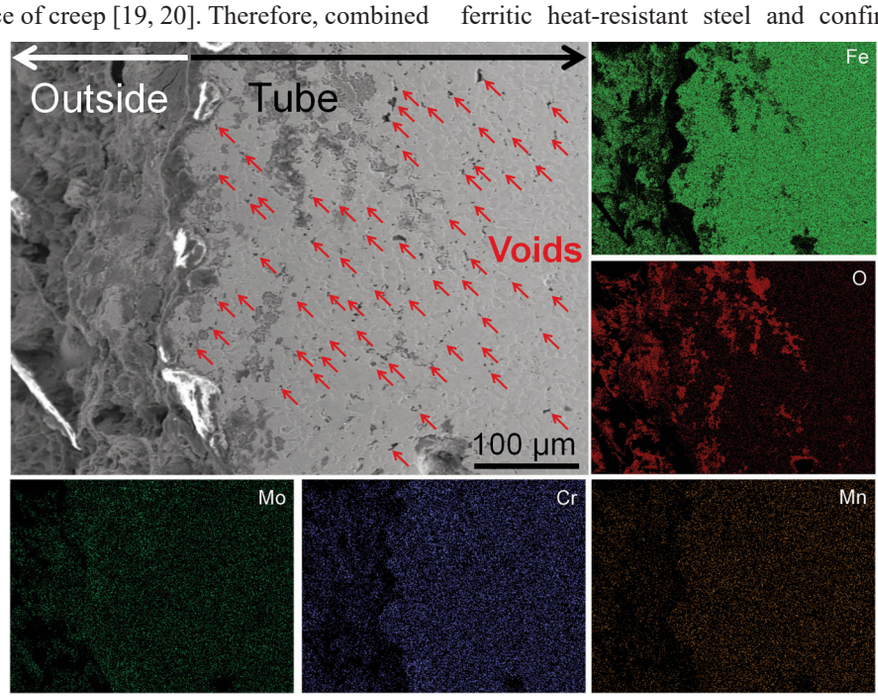

Figure 4. *SEM and EDS mapping analysis of the cross-section near the outside of the superheater tube failure position*

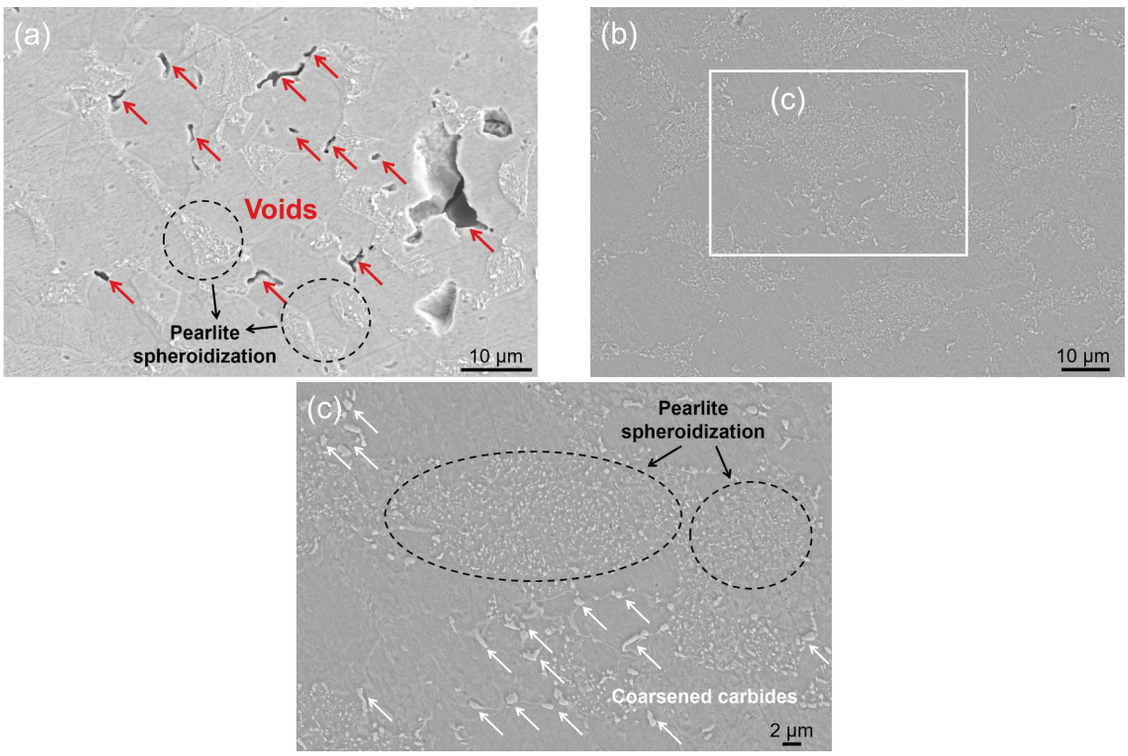

Figure 5. *High-magnification SEM image at the failure position of the superheater tube: (a) adjacent to the location of the crack, (b) position closer to the substrate than fig. 5(a) (slightly farther from the crack than shown in Fig. 5 (a)), (c) enlargement of frame position in fig. 5(b)*

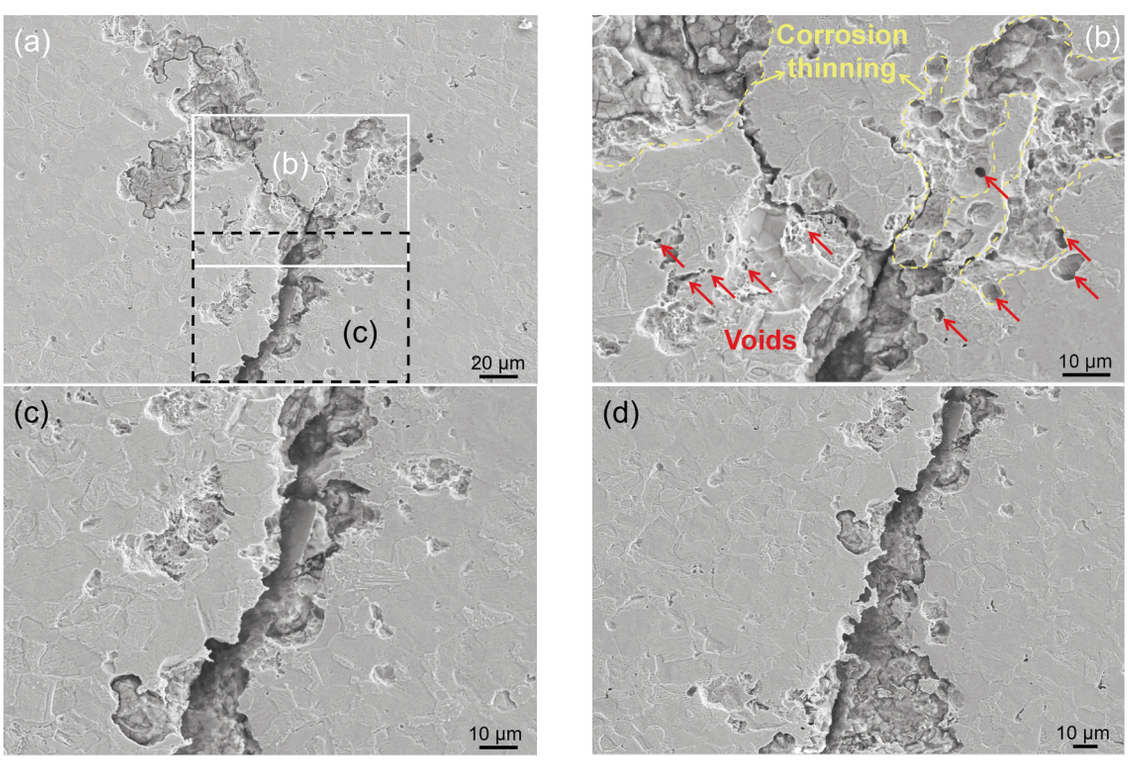

Figure 6. *SEM image of crack at the failure position of the superheater tube: (a) morphology near crack tip, (b) enlargement of the solid box position in fig. 6(a), (c) enlargement of the dashed box position in fig. 6(a), (d) extension of crack*

voids do not extend along the grain boundaries, but across them. In addition, the voids inside the grains preferentially form at the positions where pearlite spheroidization occurs, and the strength of these areas is not as strong as that of the grain boundaries, which can promote transgranular fracture. The presence of corrosion thinning can also be observed in Fig. 6(b) (indicated by the small yellow arrow), accompanied by the appearance of creep voids in the area where thinning interacts with cracks (indicated by the red thick arrow).

3.3. Corrosion products

Fig. 7 shows the SEM and EDS mapping analysis of the corrosion layer at the failure position of the superheater tube. It was found that the corroded layer is rich in Fe, O, Si, Ca, and S elements, and the matrix is rich in Fe element. In addition, O element was found near the surface layer inside the matrix, indicating the diffusion of O into the matrix, which is consistent with the phenomenon observed in Fig. 4. The presence of S element is related to the contact between the superheater tube and the flue gas or the deposition of coal ash on the superheater tube. No S element was found in the matrix, indicating that S did not diffuse into the matrix, which may be due to the low S content in the flue gas or coal ash.

The corrosion products at the failure position of the superheater tube were peeled off and ground into powder, and the phase compositions were analyzed through XRD. Fig. 8 shows the XRD detection results. It can be observed that corrosion products are composed of Fe_2O_3, Fe_3O_4, FeS and $Ca_3Fe_2(SiO_4)_3$, which is in agreement with the element distribution results of EDS analysis in Fig. 7. The presence of FeS, combined with the S in the corroded layer shown in Fig. 7, proves that the superheater tube has undergone sulfurization corrosion. It can be observed from Fig. 8 that there is amorphization in the XRD analysis of corrosion products. This can be explained by the fact that during the corrosion process, although iron oxides and iron sulfide are formed, the supersaturation required to form crystals is limited. In addition, corrosion reactions occur on the surface, and temperature and pressure conditions are not conducive to crystal formation.

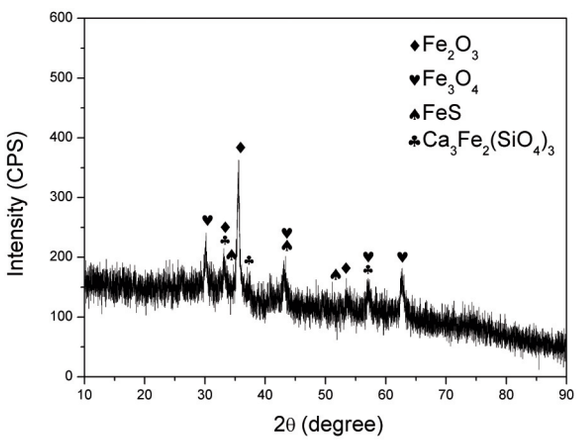

Figure 8. *XRD analysis of corrosion products powder*

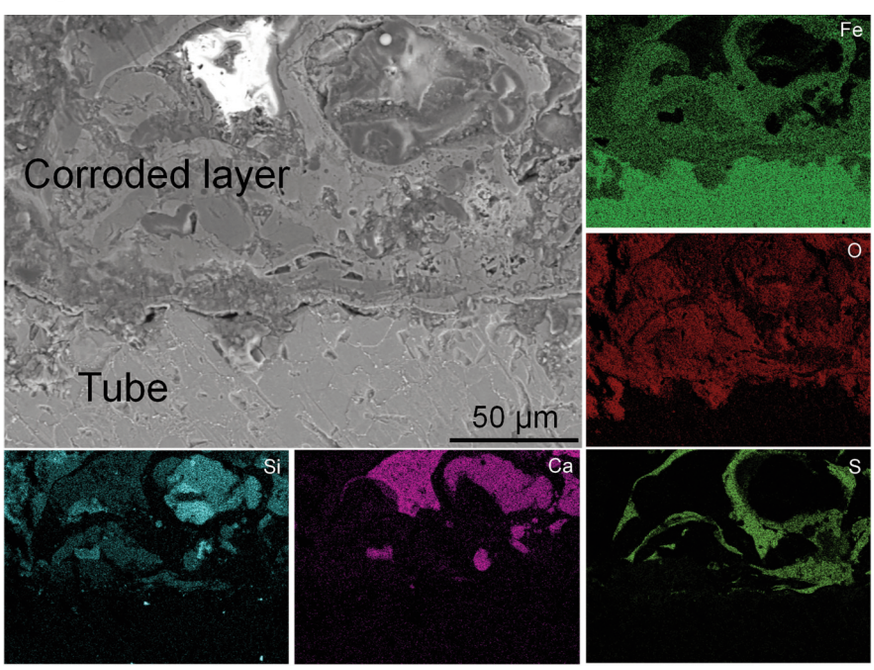

Figure 7. *SEM and EDS mapping analysis of the corroded layer at the failure position of superheater tube*

3.4. Failure cause analysis

Based on thickness measurement, microhardness testing, microstructure and corrosion product detection, as well as element distribution analysis of the failed superheater tube, the failure mechanism of the tube can be roughly inferred. The corrosion products confirmed that the superheater tube had undergone oxidation corrosion and sulfurization corrosion. By combining thickness measurement, microhardness testing, and microstructure detection, it can be concluded that the tube has undergone creep. Therefore, the failure mode of the superheater tube is the combined effect of corrosion (oxidation corrosion and sulfurization corrosion) and creep. The specific reasons are as follows:

(i) The explanation for the failure of the superheater tube caused by corrosion is as follows. Corrosion causes continuous thinning of the superheater tube during service. This can be explained by the fact that sulfides have the most crystal defects and the highest PBR (Pilling-Bedworth ratio) value in sulfides, oxides and metal substrates, and they are usually loose and porous [22-24]. During the corrosion process, sulfides will be peeled off from the corrosion layer and substrate due to different coefficients of thermal expansion [25]. With the extension of operation time, the difference in volume changes between sulfides, oxides and metal substrate increases, making it easier for the corrosion layer to come away, thereby accelerating corrosion and further thinning the superheater tube. In addition, the thermal conductivity of oxides is much lower than that of metals. For example, the thermal conductivity of Fe_3O_4 is 0.592 W/m °C, while that of ASTM A213-T12 steel is 33 W/m °C [26]. The corrosion layer mainly composed of oxides that have not peeled off from the tube will locally increase the heating temperature of the tube. This will lead to pearlite spheroidization in the microstructure of the region, resulting in a decrease in strength.

(ii) The reason for the failure of the superheater tube caused by creep is that the local overheating of the tube and an increase in loop stress of the tube. The specific analysis is as follows.

The correlation between the hardness (HV) and Larsen-Miller parameter (P) of ASTM A213-T12 steel can be expressed as [27]:

$$Hardness\ (HV) = 595.453 - 0.012603P \quad (1)$$

The Larsen-Miller parameters (P) for the normal and failed positions can be obtained by substituting the hardness (170 HV) of the normal position and the hardness (134 HV) of the failed position of the superheater tube measured in Section 3.2 into equation (1), with values of 33758 and 36615, respectively.

In addition, temperature and time can be correlated by the following equation in the Larson-Miller method [28]:

$$P = (1.8T + 492) \cdot (C + \log t) \quad (2)$$

Where T is the temperature (in degrees Celsius), t is the operating time (in hours), and C is a constant equal to 20. For the superheater tube's normal position, by substituting the Larsen Miller parameters (P) obtained from equation (1) and operating temperature (500 °C) into equation (2), the operating time of the normal tube can be calculated to be 17800 hours. The operating time at the failure position of the superheater tube is 283 days (6800 hours). By substituting the operating time of the failure position and the Larsen Miller parameters (P) obtained from equation (1) into equation (2), the operating temperature of the failure position is determined to be 580 °C. This indicates that the temperature at the failure position is significantly higher than the normal operating temperature. Therefore, pearlite spheroidization and numerous creep pores were observed at the failure position of the superheater tube, as shown in Fig. 4 and Fig. 5.

Loop stress (σ_h) generated by creep can be determined as [29]:

$$\sigma_h = p(r + 0.5h)/h \quad (3)$$

Where p represents the internal pressure of the tube during operation (in MPa), and r and h represent the inner radius and wall thickness of the tube (in mm), respectively. By substituting the average steam pressure of 12.5 MPa during the operation of the superheater tube and the size parameters of the normal position of the tube into equation (3), the loop stress value can be calculated as 26.7 MPa. For the failure position, the thickness of the tube is reduced to 2.88 mm. Assuming that the inner diameter of the tube remains unchanged at the time of failure, the loop stress value is 49.7 MPa. This indicates that the loop stress at the failure position is much higher than that at the normal position. In addition, Table 2 shows the maximum allowable stress of ASTM A213-T12 steel at different operating temperatures [30]. It can be found that the loop stress related to the operating temperature during tube failure is higher than the maximum allowable stress value at that temperature.

Table 2. *The maximum allowable stress of ASTM A213-T12 seamless tube at different operating temperatures [30]*

Operating temperature (°C)	477.78	505.56	533.33	561.11	588.89
Maximum allowable stress (MPa)	55.16	39.30	26.20	16.55	9.65

4. Conclusions

This article examines the failure behavior of ASTM A213-T12 steel superheater tubes during service. The following conclusions can be drawn:

(1) The cause of failure of ASTM A213-T12 steel is a combination of oxidation corrosion, sulfur corrosion, and creep.

(2) The thickness of ASTM A213-T12 steel superheater tube is reduced by oxidation corrosion and sulfur corrosion.

(3) The localized overheating and the increase of loop stress lead to a decrease in the creep resistance of ASTM A213-T12 steel superheater tubes.

Based on the research results of this paper, the following preventive measures are recommended:

(1) Direct impingement of flue gas on pipelines should be avoided.

(2) High-quality fuels with low sulfur content are used.

(3) Regular ash removal for tubes should be considered.

(4) Protective coating of the tube surface may be considered.

Acknowledgements

This work was financially supported by the Science&Technology Development Fund of Tianjin Education Commission for Higher Education (No. 2023KJ250).

Authorship contributions

Jianguo Chen: Paper writing, Supervision. Ji Dong: Investigation. Hanwen Zhang: Investigation. Yaxin Huang: Investigation. Qingjun Ma: Formal analysis. Yushun Wei: Formal analysis. Hengsheng Ma: Formal analysis.

Data availability

All data generated or analyzed during this work are included in this published article.

Conflicts of interests

We declare that we have no known competing financial interests that could have appeared to influence the work reported in this paper.

References

[1] P.C. Dsilva, S. Bhat, J. Banappanavar, K.G. Kodancha, S.R. Hegde, Premature failure of superheater tubes in a fertilizer plant, Engineering Failure Analysis, 121 (2021) 105152. https://doi.org/DOI:10.1016/j.engfailanal.2020.105152

[2] R. Viswanathan, W. Bakker, Materials for ultrasupercritical coal power plants-boiler materials: part 1, Journal of Materials Engineering and Performance, 10 (2001) 81-95. https://doi.org/DOI:10.1361/105994901770345394

[3] S. Zangeneh, H.R. Lashgari, F. Pahnane, M. Mehdizadeh, F. Panjehaein, M. Mojtahedi, R. Bakhtiari, Failure analysis of A213 TP347H superheater outlet tube in A 320-MW power plant, Journal of Failure Analysis and Prevention, 22 (2022) 1872-1882. https://doi.org/DOI:10.1007/s11668-022-01474-x

[4] P. Kochmański, S. Fryska, A.E. Kochmańska, Failure analysis of steam superheater boiler tube made of ASTM T22 steel, Engineering Failure Analysis, 162 (2024) 108366. https://doi.org/DOI:10.1016/j.engfailanal.2024.108366

[5] Z. Wang, J Zhao, H Cai, G Chai, Failure analysis of a 12Cr1MoV superheater tube after 280,000 h of service, Nuclear Materials and Energy, 40 (2024) 101707. https://doi.org/DOI:10.1016/j.nme.2024.101707

[6] T. Liu, T. Jiang, J. Zhong, K. Guan, Z. Wang, F. Arjmand, Failure analysis of sulphidation-oxidation corrosion of Incoloy 800HT superheater tube, Engineering Failure Analysis, 142 (2022) 106798. https://doi.org/DOI:10.1016/j.engfailanal.2024.108366

[7] Y. Li, H. Chen, Z. Pan, H. Liang, Z. Wang, Z. Feng, Z. Li, Y. Kuang, Failure analysis of superheater tubes in an air quenching cooler waste heat boiler, Engineering Failure Analysis, 131 (2022) 105869. https://doi.org/DOI:10.1016/j.engfailanal.2021.105869

[8] R. Viswanathan, K. Coleman, U. Rao, Materials for ultra-supercritical coal-fired power plant boilers, International Journal of Pressure Vessels and Piping, 83 (2016) 778-783. https://doi.org/DOI:10.1016/j.ijpvp.2006.08.006

[9] F. Chen, W. Zhang, K. Zhang, Q. Yang, X. Wang, C. Zhou, Low cycle fatigue and creep-fatigue interaction behavior of 2.25CrMoV steel at high temperature, Journal of Materials Research and Technology, 28 (2024) 3153-3165. https://doi.org/DOI:10.1016/j.jmrt.2023.12.233

[10] F. Masuyama, History of power plants and progress in heat resistant steels, ISIJ International, 41 (2001) 612-625. https://doi.org/DOI:10.2355/isijinternational.41.612

[11] D.N. Adnyana, Case study on fireside erosion of platen superheater boiler tubes of a coal-fired power plant, Journal of Failure Analysis and Prevention, 22 (2022) 1578-1589. https://doi.org/DOI:10.1007/s11668-022-01450-5

[12] M. Sabouria, H.R. Faridi, Investigation on corrosion failure of Cr-Mo P11 grade pipe in primary section of a superheated steam generation system, High Temperature, 55 (2017) 139-144. https://doi.org/DOI:10.1134/S0018151X17010205

[13] J.C.M. Farrar, The Alloy Tree, A Guide to Low-Alloy Steels, Stainless Steels and Nickel-Base Alloys, CRC Press, Boca Raton, Boston, New York and Washington DC, 2004, p.7.

[14] ASTM A213/A213M-23, Standard Specification for Seamless Ferritic and Austenitic Alloy-Steel Boiler, Superheater, and Heat-Exchanger Tubes, ASTM

International, West Conshohocken, United States, 2023.

[15] B. Karpe, K. Prijatelj, M. Bizjak, T. Kosec, Corrosion properties of aluminized 16Mo3 steel, Journal of Mining and Metallurgy, Section B: Metallurgy, 59 (2023) 91-100. https://doi.org/DOI:10.2298/JMMB220927008K

[16] A. Bahrami, A. Mohammadnejad, M.K. Khouzani, M. Pouradineh, V. Esmaeili, Stress relaxation cracking failure in a high pressure steam pipeline in an ammonia plant, International Journal of Pressure Vessels and Piping, 194 (2021) 104542. https://doi.org/DOI:10.1016/j.ijpvp.2021.104542

[17] S. Fintová, I. Kuběna, M. Jarý, N. Luptáková, L. Stratil, F. Šiška, J. Svoboda, Creep properties of heat-treated Fe-Al-O ODS alloy, Kovove Materialy-Metallic Materials, 59 (2021) 39-50. https://doi.org/DOI:10.4149/km_2021_1_39

[18] D.R.H. Jones, Creep failures of overheated boiler, superheater and reformer tubes, Engineering Failure Analysis, 11 (2004) 873-893. https://doi.org/DOI:10.1016/j.engfailanal.2004.03.001

[19] J.G. Chen, Y.C. Liu, Y.T. Xiao, Y.H. Liu, C.X. Liu, H.J. Li, Improvement of high-temperature mechanical properties of low-carbon RAFM steel by MX precipitates, Acta Metallurgica Sinica (English Letters), 31 (2018) 706-712. https://doi.org/DOI:10.1007/s40195-018-0703-y

[20] Z. Lyu, R. Kannan, N. Saini, J. Li, L. Li, Degradation of a Cr-Mo steel by carbide precipitation over long-term service, Materials Science and Engineering A, 898 (2024) 146354. https://doi.org/DOI:10.1016/j.msea.2024.146354

[21] X.S. Zhou, Y.C. Liu, C.X. Liu, B.Q. Ning, Evolution of creep damage in a modified ferritic heat resistant steel with excellent short-term creep performance and its oxide layer characteristic, Materials Science and Engineering A, 608 (2014) 46-52. https://doi.org/DOI:10.1016/j.msea.2014.04.075

[22] Z. Liang, M. Yu, Q. Zhao, Investigation of fireside corrosion of austenitic heat-resistant steel 10Cr18Ni9Cu3NbN in ultra-supercritical power plants, Engineering Failure Analysis, 100 (2019) 180-191. https://doi.org/DOI:10.1016/j.engfailanal.2019.02.048

[23] C. Wei, Z.J. Wang, J.G. Chen, Sulfuration corrosion failure analysis of Inconel 600 alloy heater sleeve in high-temperature flue gas, Engineering Failure Analysis, 135 (2022) 106111. https://doi.org/DOI:10.1016/j.engfailanal.2022.106111

[24] X. Li, Corrosion behaviours of two nickel-based coatings in H_2S-containing environments, Surface and Coatings Technology, 183 (2004) 212-215. https://doi.org/DOI:10.1016/j.surfcoat.2003.09.067

[25] K. Luo, C. Li, F. Xue, Y. Liu, L. Zhang, G. Zhang, in High Performance Structural Materials (Y. Han Editor), Springer, Singapore, 2018, p.557-656.

[26] A. Firouzeh, K. Ranjbar, S.M. Lari Baghal, A. Heidari Kaidan, E. Mohemi, Failure assessment of ASTM A213-T12 superheater boiler tubes in a natural gas liquid plant, Engineering Failure Analysis, 89 (2018) 15-27. https://doi.org/DOI:10.1016/j.engfailanal.2018.03.005

[27] J. Purbolaksono, J. Ahmad, L.C. Beng, A.Z. Rashid, A. Khinani, A.A. Ali, Failure analysis on a primary superheater tube of a power plant, Engineering Failure Analysis, 17 (2010) 158-167. https://doi.org/DOI:10.1016/j.engfailanal.2009.04.017

[28] M.M. Rahman, J. Purbolaksono, J. Ahmad, Root cause failure analysis of a division wall superheater tube of a coal-fired power station, Engineering Failure Analysis, 17 (2010) 1490-1494. https://doi.org/DOI:10.1016/j.engfailanal.2010.05.005

[29] H. Shokouhmand, B. Ghadimi, R. Espanani, Failure analysis and retrofitting of superheater tubes in utility boiler, Engineering Failure Analysis, 50 (2015) 20-28. https://doi.org/DOI:10.1016/j.engfailanal.2015.01.003

[30] H.S. Babak, F.N. Hossein, N.S. Masoud, A. Pooria, N. Farzad, Failure analysis of a superheater tube ruptured in a power plant boiler: main causes and preventive strategies, Engineering Failure Analysis, 98 (2019) 131-140. https://doi.org/DOI:10.1016/j.engfailanal.2019.01.016

ANALIZA UZROKA PREURANJENOG PUCANJA CEVI PREGREJAČA OD ASTM A213-T12

J.-G. Chen [a, *], J. Dong [a], H.-W. Zhang [b], Y.-X. Huang [b], Q.-J. Ma [b], Y.-S. Wei [b], H.-S. Ma [c]

[a] Fakultet mašinstva, Kinesko-nemački univerzitet primenjenih nauka u Tianjinu, Tian jin, NR Kina
[b] Institut za inspekciju specijalne opreme Tianjin, Tianjin, NR Kina
[c] Grupa za materijale za zavarivanje Tianjin Bridge, Tianjin, NR Kina

Apstrakt

U ovom radu proučavano je ponašanje cevi pregrejača od čelika ASTM A213-T12 u slučaju preloma. Mikrostruktura i tvrdoća na različitim mestima na cevi, raspodela elemenata na mestu pucanja, kao i morfologija i fazni sastav korozionog sloja analizirani su pomoću optičke mikroskopije (OM), uređaja za mikrotvrdoću, skenirajuće elektronske mikroskopije (SEM) i rendgenske difraktometrije (XRD). Rezultati pokazuju da dolazi do sferoidizacije perlita na mestu pucanja, a tvrdoća je značajno smanjena u poređenju sa normalnim delom cevi. Prelom je usko povezan sa korozijom i puzanjem. S jedne strane, na spoljnjem sloju cevi pregrejača javljaju se sumporna i oksidaciona korozija, što značajno smanjuje debljinu cevi. S druge strane, otpornost cevi na puzanje je značajno smanjena zbog proređivanja zida. Na mestu preloma, mikrostruktura pokazuje prisustvo brojnih šupljina nastalih usled puzanja. Istovremeno, može doći do difuzije kiseonika u šupljine čime se podstiče oksidaciona korozija.

Ključne reči: *Cev pregrejača; Analiza preloma; Puzanje; Korozija; Mikrostruktura*